Electronic Supplementary Material (ESI) for Chemical Communications.

Metal-to-metal electron transfer in a cyanido-bridged $\{Fe_2Co_2\}$ square complex followed by X-ray diffraction and absorption techniques

Corine Mathonière,*[ab] Dmitri Mitcov,[a] Evangelia Koumousi,[ab] Daniel Amorin-Rosario,[a] Pierre Dechambenoit,[a] Sadaf Fatima Jafri,[c] Philippe Sainctavit,[c] Christophe Cartier dit Moulin,[d] Loïc Toupet,[e] Elzbieta Trzop,[e] Eric Collet,[e] Marie-Anne Arrio,[c] Andrei Rogalev,[f] Fabrice Wilhelm[f] and Rodolphe Clérac*[a]

[a.] *Univ. Bordeaux, CNRS, Centre de Recherche Paul Pascal, CRPP, UMR 5031, 33600 Pessac, France. E-mail: corine.mathoniere@u-bordeaux.fr & rodolphe.clerac@u-bordeaux.fr*

[b.] *Univ. Bordeaux, CNRS, Bordeaux INP, ICMCB, UMR 5026, 33600 Pessac, France.*

[c.] *Institut de Minéralogie, de Physique des Matériaux et de Cosmochimie, CNRS UMR7590, Sorbonne Université, MNHN, 75252 Paris Cedex 5, France.*

[d.] *Institut Parisien de Chimie Moléculaire, IPCM, Sorbonne Université, CNRS, F-75005 Paris, France.*

[e.] *Univ. Rennes, CNRS, Institut de Physique de Rennes (IPR) – UMR 6251, F-35000 Rennes, France.*

[f.] *ESRF – The European Synchrotron, 38043 Grenoble, France.*

Experimental section

Synthesis of {[(Tp*)Fe(CN)$_3$]$_2$[Co(bpy^{Me})$_2$]$_2$}(OTf)$_2$•2DMF•H$_2$O (**1**). The synthesis of **1** has been carried out following the reported procedure by Siretanu et al.[1] [NEt$_4$][(Tp*)Fe(CN)$_3$]·2H$_2$O (168 mg, 0.3 mmol) was reacted with Co(OTf)$_2$ (107 mg, 0.3 mmol) in 5 mL of wet DMF under argon to afford a red solution that was allowed to stir for 2 hours. Then 4,4′-dimethyl-2,2′-bipyridine (diMebpy; 114 mg, 0.6 mmol) was added and the mixture was stirred for 20 minutes and filtered. Dark red crystals (0.23 g, 70 %) were obtained by slow diffusion of diethyl ether into the DMF solution. Prior to the different measurements reported in this work, the compound has been characterized by elemental analysis, and standard magnetic measurements. Elemental analysis – Calc. (Found) $C_{92}H_{108}B_2Co_2F_6Fe_2N_{28}O_9S_2$: C, 50.70 (50.36); H, 5.00 (4.94); N, 18.00 (18.13). Selected FT-IR data (ATR, cm^{-1}): 2926 (w), 2857 (w), 2546 (w), 2151, 2116 (w), 1664 (s), 1614 (s), 1541 (s), 1444 (s), 1414 (s), 1385 (s), 1369 (s), 1263 (vs), 1202 (s), 1138 (s), 1062 (s), 1031 (s), 824 (s), 793 (s), 635 (vs), 572 (s).

Single crystal X-ray diffraction. Structural investigations at thermal equilibrium (80 and 240 K) and under continuous light irradiation at 80 K were carried out with an Xcalibur 3 four-circle diffractometer (Oxford Diffraction) equipped with a 2D sapphire 3 CCD detector with Mo K_α radiation (λ = 0.71073 Å) on a single crystal covered with immersion oil to avoid solvent loss (with typical sizes around 100 × 150 × 200 μm^3). A nitrogen-flow cryostat was used with a temperature stability of 0.1 K. Complete crystallographic data were collected both at thermal equilibrium at 80 K, 240 K and under light irradiation at 80 K. The structures were solved with SIR-97[2] and refined with SHELXL[3] and typical results of the structure refinement of the stable and photoinduced states gave final R_1 factor between 0.0802 and 0.0843. In addition, partial data sets (10 minutes) were collected for investigating the lattice parameters as (i) a function of the temperature (between each temperature step, the sample was cooled down at 1 K min^{-1}), as well as (ii) a function of the light irradiation time at 80 K. During the X-ray diffraction measurements of the {Fe$^{II}_2$Co$^{III}_2$} phase, its lattice parameters and global structure at 80 K stay unchanged. X-ray-induced electron transfer using Mo radiation at 17 479 eV was not observed during the different X-ray diffraction data collection. It is worth mentioning that is contrasting with the fast evolution of lattice parameters and overall structure under white light irradiation. Structures were deposited in the Cambridge Structure Database (CCDC 2182862-2182864).

X-ray absorption spectroscopy (XAS). XAS at the *K*-edge of Fe (7.1 keV) and Co (7.7 keV) were recorded at ID12 beamline of the European Synchrotron Radiation Facility (ESRF) using total fluorescence yield detection mode. In the required photon energy range, the fundamental harmonic of helical undulator of APPLE-II type was used and the incident X-ray flux was further attenuated by about a factor of 10 by

inserting Al foils with total thickness of 150 μm. The advantage of using helical undulator is that the content of the higher order harmonics is strongly reduced, since only the fundamental harmonic is emitted on the undulator axis. The X-ray beam was further monochromatized using a fixed-exit double-crystal monochromator equipped with a pair of Si(111) crystals. The energy scale of the monochromator was calibrated using a pre-edge feature of the *K*-edge spectra of metallic titanium at 4.9655 keV. Given the extremely low emittance of the source, the energy resolution was found to agree quite well with theoretical predictions for perfect Si crystals: 1.05 eV at the iron *K*-edge and 1.15 eV at the cobalt *K*-edge. In all cases, the instrumental resolution was better than the respective atomic natural widths:[4] 1.25 and 1.33 eV. As the polycrystalline sample of **1** is sensitive to solvent loss, the X-ray absorption spectra were collected using a vacuum tight cell where the crystals of **1** are immobilized in a silicon oil and protected with a 13 μm thick kapton window. The sample holder was attached to a cold finger of a constant flow He cryostat allowing measurements in the 3 – 300 K temperature range. In the required photon energy range, the second harmonic of Helios-II type of undulator was used and the incident X-ray flux was further adjusted by inserting thin Al foils. A careful analysis of the Total Fluorescence yield as a function of temperature has been performed and the experimental data have been corrected to account for the background fluorescence of all elements of the sample, the angle of incidence of the X-ray beam, and the solid angle of the fluorescence detector, that was slightly varying due to the contraction of the cold finger of the cryostat. For the sake of comparison, the corrected spectra were systematically normalized to the edge jump.

Table S1. Crystallographic data for **1** at various temperatures.

Temperature	240 K	80 K before light irradiation	80 K after light irradiation
Crystal color	dark red	dark green	dark red
Moiety formula	$C_{84}H_{92}B_2Co_2Fe_2N_{26}$, $2(CF_3O_3S)$, $2(C_3H_7NO)$, (H_2O)		
Empirical formula	$C_{92}H_{108}B_2Co_2F_6Fe_2N_{28}O_9S_2$		
Formula weight, g mol^{-1}	2179.32		
Crystal system	Triclinic		
Space group	$P\bar{1}$		
Wavelength, Å	0.71073		
a, Å	13.5817(9)	13.2457(11)	13.3992(11)
b, Å	14.0463(8)	13.8227(9)	13.9160(9)
c, Å	14.9259(10)	14.7690(12)	14.8696(12)
α, °	69.516(6)	69.953(7)	69.246(7)
β, °	89.648(6)	87.972(7)	89.144(7)
γ, °	73.040(6)	71.580(7)	72.923(7)
V, Å^3	2536.7(3)	2402.1(3)	2466.1(4)
Z	1		
ρ_{calcd}, g/cm^3	1.427	1.507	1.467
μ, mm^{-1}	0.723	0.764	0.744
Reflections collected	17159	16164	19356
Independent reflections	8913	8442	8673
R_1[a]	0.0802	0.0818	0.0843
wR_2[a]	0.1605	0.1649	0.1785
GoF[a]	1.001	1.001	1.019
Selected bond distances (Å)			
Co(1)-N(7)	2.089(6)	1.916(6)	2.094(7)
Co(1)-N(9)	2.106(6)	1.888(6)	2.101(6)
Co(1)-N(10)	2.115(6)	1.926(6)	2.120(7)
Co(1)-N(11)	2.149 (6)	1.945(6)	2.154(6)
Co(1)-N(12)	2.137(6)	1.946(7)	2.112(6)
Co(1)-N(13)	2.114(7)	1.939 (7)	2.098(7)
Fe(1)-C(16)	1.914(8)	1.857(8)	1.923(8)
Fe(1)-C(17)	1.929(8)	1.900(8)	1.922(8)
Fe(1)-C(18)	1.925(7)	1.870(8)	1.931(8)
Fe(1)-N(1)	1.999(6)	2.048(6)	1.999(6)
Fe(1)-N(3)	1.997(6)	2.027(6)	1.989(7)
Fe(1)-N(5)	1.989(6)	2.053(6)	1.971(7)
Selected bond angles (°)			
N(7)-Co(1)-N(9)	90.7(2)	90.1(3)	89.8(2)
N(7)-Co(1)-N(10)	93.3(2)	93.0(3)	92.5(3)
N(7)-Co(1)-N(12)	92.4(2)	90.6(2)	91.6(2)
N(7)-Co(1)-N(13)	96.2(2)	91.9(3)	96.3(2)
N(9)-Co(1)-N(10)	89.1(2)	88.3(3)	88.3(2)
N(9)-Co(1)-N(11)	88.6(2)	88.6(2)	88.8(2)
N(9)-Co(1)-N(13)	96.4(3)	94.3(3)	97.0(3)
N(10)-Co(1)-N(11)	76.0(2)	82.6(3)	76.6(3)
N(10)-Co(1)-N(12)	97.2(2)	94.7(3)	97.2(2)
N(12)-Co(1)-N(11)	89.7(2)	90.9(2)	90.8(2)
N(13)-Co(1)-N(11)	94.5(2)	92.6(3)	94.6(3)
N(13)-Co(1)-N(12)	76.7(3)	82.7(3)	77.3(3)
C(16)-N(7)-Co(1)	164.7(6)	164.6(7)	163.8(6)
C(18)-N(9)-Co(1)	165.3(6)	167.2(6)	163.3(6)
C(16)-Fe(1)-C(17)	84.1(3)	85.0(3)	83.0(3)
C(16)-Fe(1)-C(18)	91.1(3)	92.4(3)	91.9(3)
N(7)-C(16)-Fe(1)	178.8(7)	177.7(7)	179.1(7)
N(8)-C(17)-Fe(1)	173.6(7)	173.9(7)	173.2(7)
N(9)-C(18)-Fe(1)	174.5(6)	175.2(7)	175.0(7)

[a] $I > 2\sigma(I)$, $R_1 = \Sigma(||F_o| - |F_c||)/\Sigma|F_o|$. $wR_2 = \{\Sigma[w(F_o^2 - F_c^2)^2]/\Sigma[w(F_o^2)^2]\}^{1/2}$. GoF (goodness of fit on F^2) = $\{\Sigma[w(F_o^2 - F_c^2)^2]/(n\text{-}p)\}^{1/2}$, where *n* is the number of reflections and *p* is the total number of refined parameters.

Table S2. Average metal-to-ligand bond lengths, metal-to-metal distances and deformation of the Co coordination sphere for **1** under different experimental conditions.

	(1)		
	240 K	**80 K**	**80 K**
	$\{Fe^{III}_2Co^{II}_2\}$	**before light irradiation $\{Fe^{II}_2Co^{III}_2\}$**	**after light irradiation $\{Fe^{III}_2Co^{II}_2\}$**
<Fe-C>, Å	1.923	1.876	1.925
<Fe-N>, Å	1.995	2.043	1.986
<Co-N>, Å	2.118	1.927	2.113
Fe(1)···Co(1), Å	5.108	4.891	5.113
Fe(1)···Co(1)', Å	5.114	4.896	5.099
Fe···Fe, Å	7.154	6.785	7.088
Co···Co, Å	7.301	7.052	7.351
Σ(N-Co-N)[a], °	60.6	35.9	59.2

[a] $\sum = \sum_{i=1}^{12}|90 - \varphi_i|$ *where* ϕ_i *are N-Co-N bond angles*

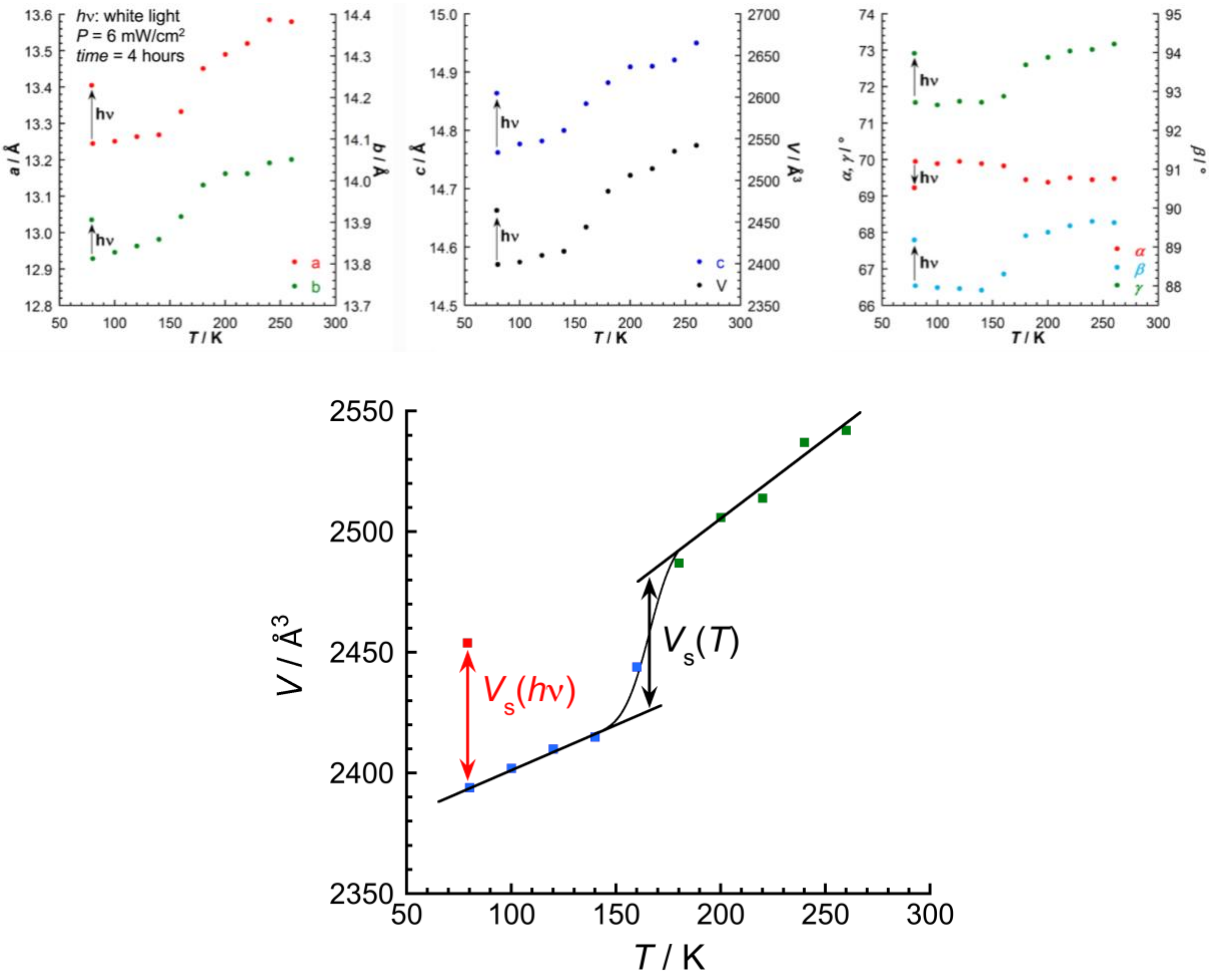

Figure S1. (top) Thermal evolution of lattice parameters for **1** during cooling process. For each temperature, the measurement took 10 minutes. In between each temperature step, the sample was cooled down at 1 K min^{-1}. (bottom) The volume change is attributed to the thermally ($V_s(T)$) or optically ($V_s(h\nu)$) induced ET.

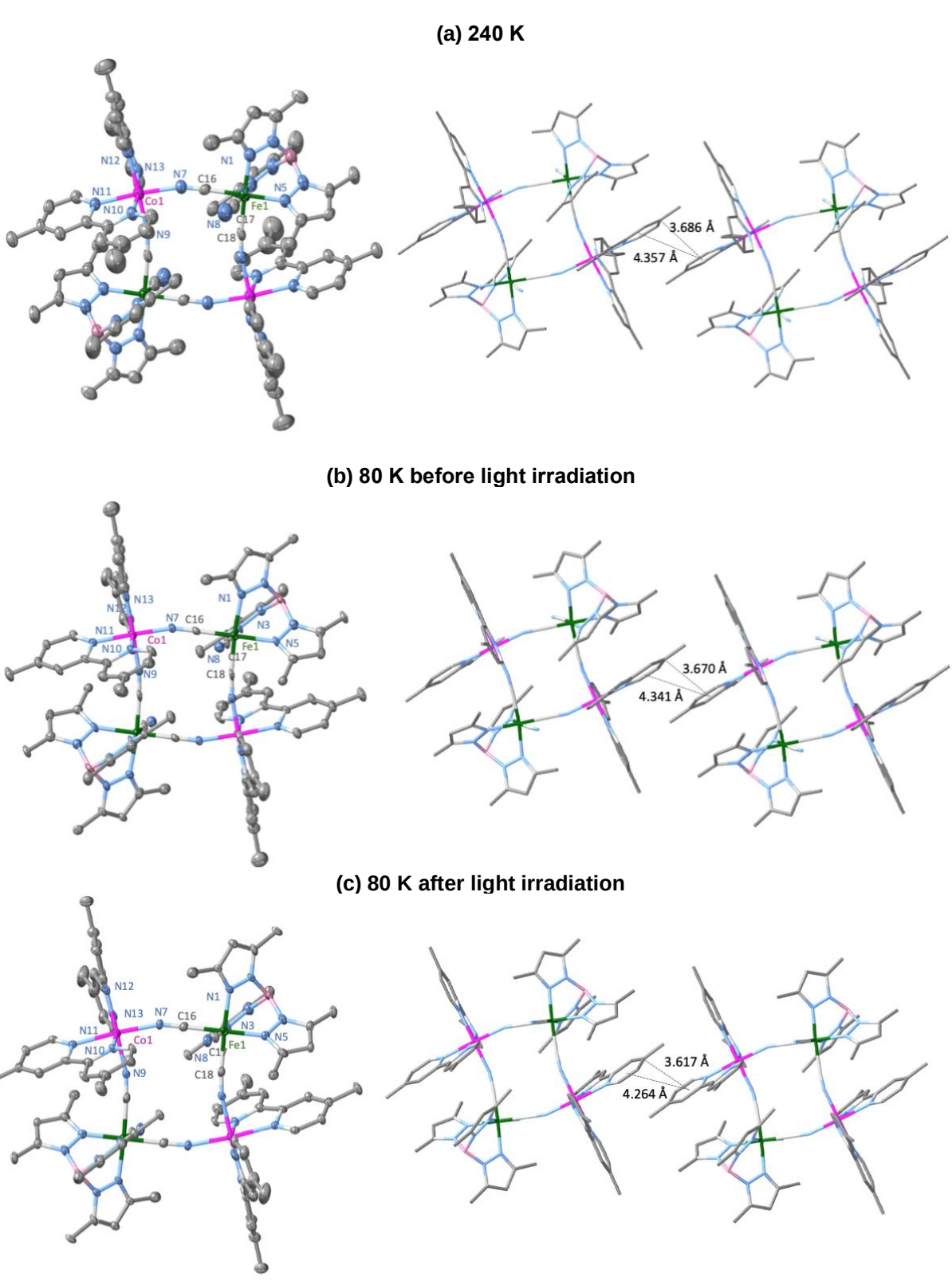

Figure S2. (left) Cationic portion of **1** in its: (a) high temperature phase at 240 K; (b) low temperature phase collected at 80 K; and (c) photo-induced metastable paramagnetic phase at 80 K. Thermal ellipsoids are at 50% probability. (right) Packing arrangement illustrating π-π interactions present between adjacent complexes along the crystallographic *b*-direction under different experimental conditions. All anions, lattice solvent and hydrogen atoms are not shown for clarity.

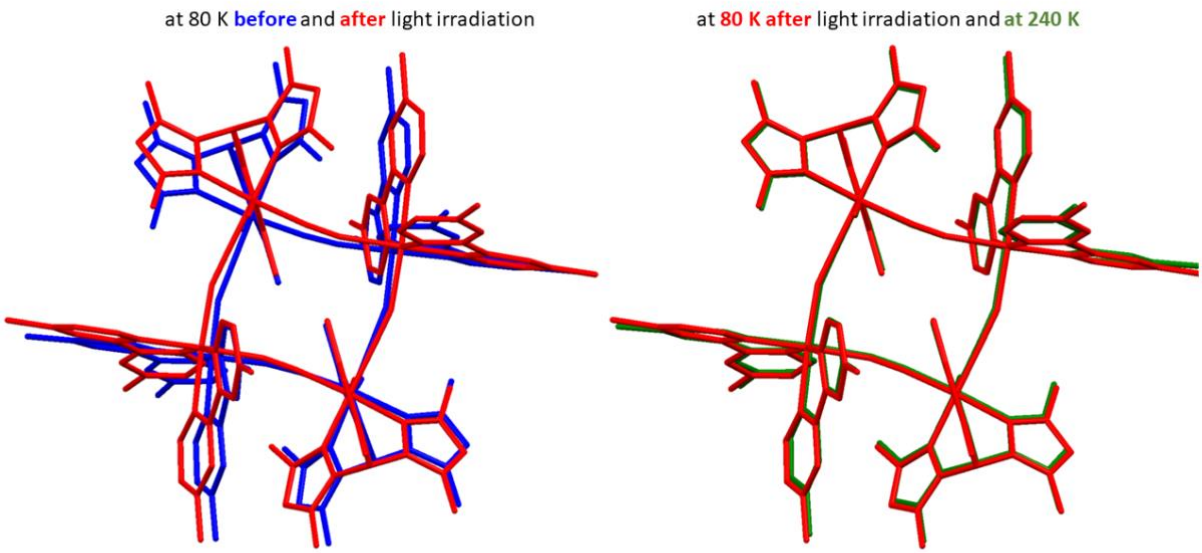

Figure S3. Superposed views of the cationic $\{[(Tp^*)Fe(CN)_3]_2[Co(bpy^{Me})_2]_2\}^{2+}$ core in **1**: (left) emphasizing the structural differences before (blue) and after (red) white light irradiation at 80 K (P = 6 mW/cm^2); (right) emphasizing the differences between the molecular structure at 240 K (green) and after white light irradiation at 80 K (red; P = 6 mW/cm^2). All anions, lattice solvent and hydrogen atoms are not shown for clarity. In addition to these intra-molecular reorganizations, the lattice contraction between the high and low temperature phases is associated with a relative motion of the molecules within the crystalline lattice. However, there is no significant change of the interactions between the free cyanide, counter anions or solvent molecules as shown on the supplementary video 3 (MOV3.mp4).

X-ray absorption spectroscopy (XAS): pre-edge analysis using Ligand Field Multiplet (LFM) calculations.

Table S3. LFM parameters (all expressed in eV except β) used in the theoretical pre-edge spectra shown in Fig. S4.

	10 *Dq*	$D\sigma$	$D\tau$	β	Δ_i	Δ_f	V_{eg}	V_{t2g}
Fe(II)	2.8	0.07	0.12	0.7	1.0	1.4	−0.8	1.8
Fe(III)	2.8	0.07	0.12	0.7	3.0	3.4	−0.8	1.8
Co(II)	1.0	-	-	0.7	-	-	-	-
Co(III)	2.2	-	-	0.7	-	-	-	-

The pre- *K*-edge spectra (Fig. S4) were calculated in the frame of the Ligand Field Multiplet (LFM) model using the codes written by T. Thole as described in references **5-8**. In the LFM approach, the pre-edge structures due to the 1s $\rightarrow$ 3d electric quadrupole transitions are described as transitions from $3d^n$ ground state to $1s^1 3d^{(n+1)}$ excited states. For the Co(II) and Co(III) metal ions, a single electronic configuration was considered (respectively $3d^7$ and $3d^6$) in O_h symmetry.**8** For the Fe(II) and Fe(III) metal ions bonded to the cyanido carbons, two configurations were considered to include Metal-to-Ligand Charge Transfer (MLCT) induced by the π back bonding of the cyanido bond ($3d^6$-$3d^5L^-$ for Fe(II) and $3d^5$-$3d^4L^-$ for Fe(III)), as described in references **9-12**. The site symmetry was simplified to C_{3v} and only 1s $\rightarrow$ 3d electric quadripole transitions were calculated. It is worth mentioning that in the real symmetry, the non-centrosymmetry of the sites allows theoretically the p-d mixing and 1s $\rightarrow$ p electric dipole transitions in the pre-edge region but this contribution was neglected as it is commonly done for 6 fold-coordinated cations. The LFM parameters used in the calculations are summarized in the Table S3.

For high-spin (HS) Co(II) site in O_h symmetry, the pre-edge features are due the transitions from the $^4T_{1g}$ d^7 HS-Co(II) ground state to the $1s^1 3d^8$ Co(II) excited states ($^4A_{2g}$, $^4T_{2g}$, $^4T_{1g}$ deriving from the ^3F spherical state and $^4T_{1g}$ coming from the ^3P spherical state).**8** In the case of the low-spin (LS) Co(III), the transitions are from the LS-d^6 ground state ($^1A_{1g}$) to the LS-$1s^1d^7$ excited state (^1E_g).**8**

For LS-Fe(III) in O_h symmetry without π back bonding, the pre-edge features are due to transitions from the LS-d^5 ground state ($^2T_{2g}$) to the LS-$1s^1d^6$ states ($^2T_{1g}$, $^2T_{2g}$, $^2T_{1g}$, $^2T_{2g}$).**13** In the C_{3v} symmetry, small splittings occur that are hardly detected with the energy resolution at the *K*-edges. We used the LFM parameters found for $[TpFe^{III}(CN)_3]^-$ building block complex.**10** The feature at higher energy (7118.8 eV) is due to the π back bonding as described for $K_3[Fe(CN)_6]$ by Lundberg *et al*.**11** The calculation leads to a $0.73|d^5> + 0.27|d^4L^->$ ground state composition and the number of 3d electrons is 4.73. For LS-Fe(II) in O_h symmetry without π back bonding, the pre-edge is due to the transitions from the LS-d^6 ground state ($^1A_{1g}$) to the LS-$1s^1d^7$ state (^1E_g).**13** The feature at higher energy (7117 eV) is due to the π back bonding as described for $K_4[Fe(CN)_6]$.**11** The calculation leads to a $0.61|d^6> + 0.39|d^5L^->$ ground state composition and the number of 3d electrons is 5.61.

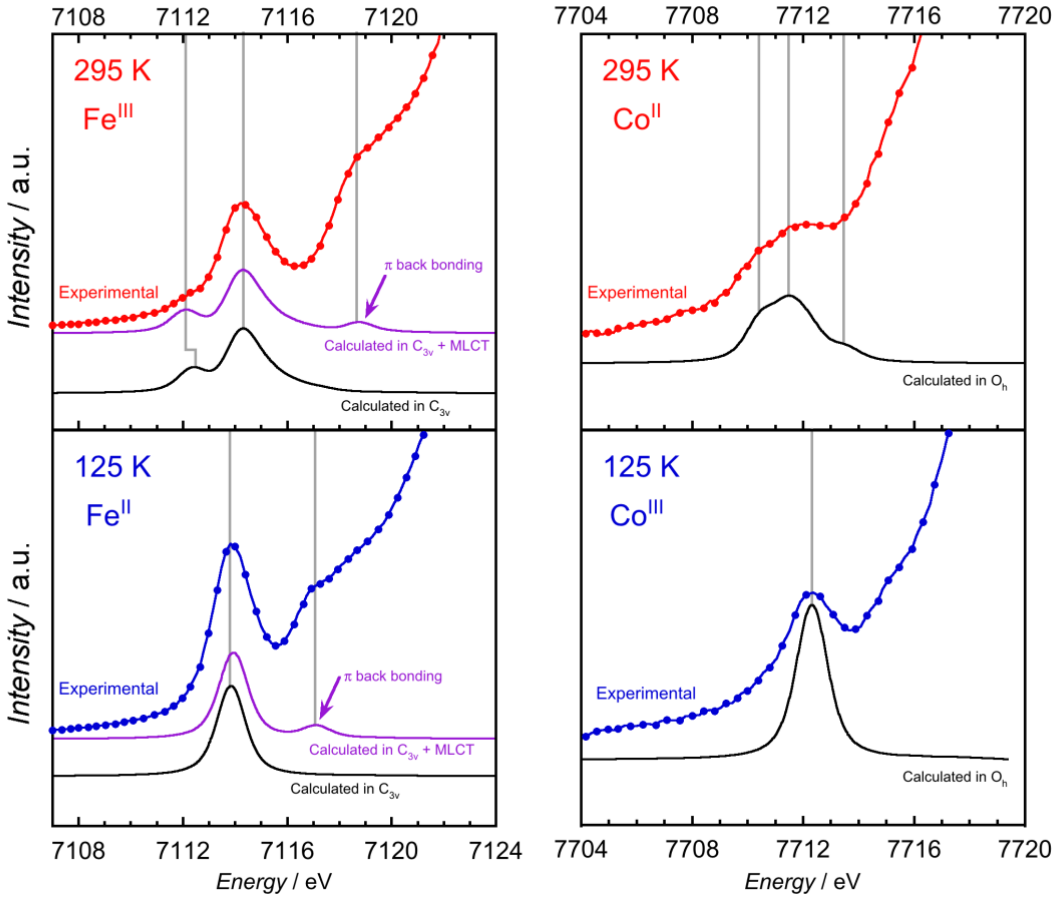

Figure S4. Pre- *K*-edges regions of **1** at 295 K (top) and 125 K (bottom) for the Fe (left) and Co (right) metal ions. Experimental spectra (red for 295 K and blue for 125 K) and theoretical spectra using the LFM calculations (see text above; in black and purple solid lines). The vertical gray lines are guides for the eyes to compare the positions of the experimental and theoretical transitions.

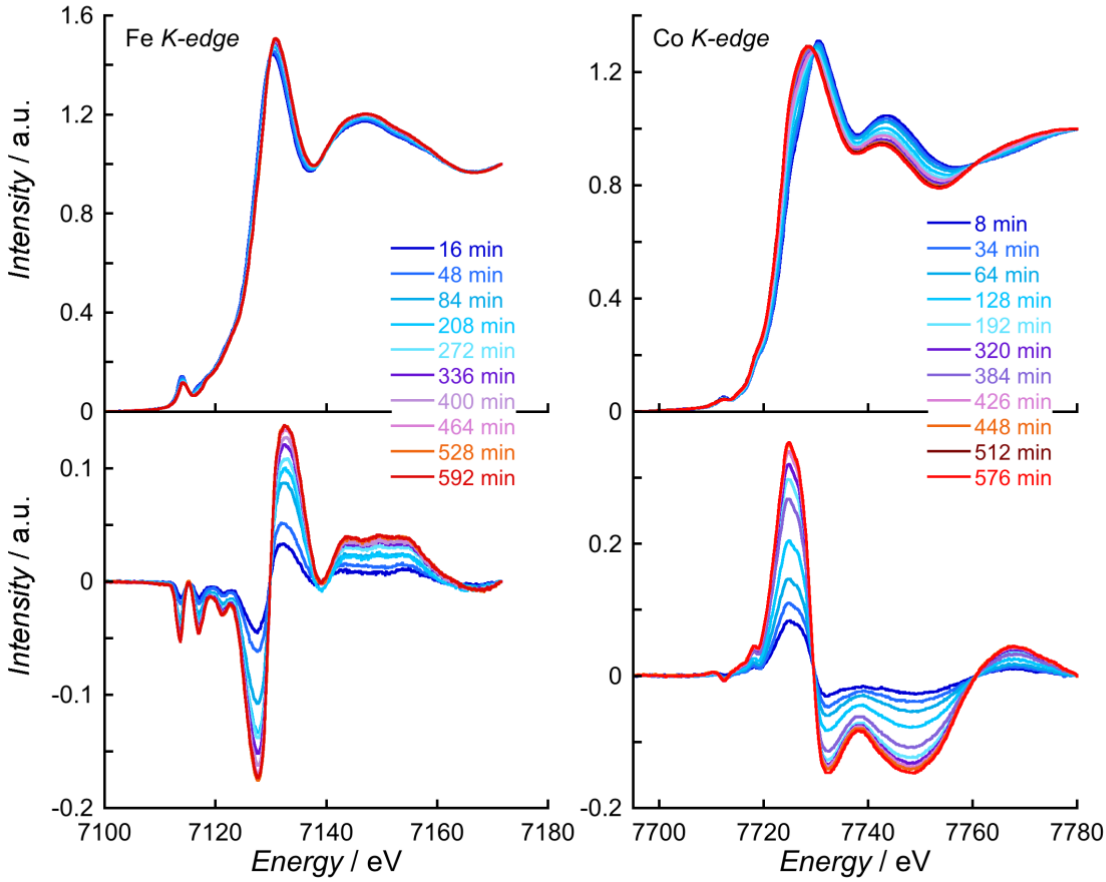

Figure S5. (top) X-ray absorption spectra of **1** at 3 K during the X-ray irradiation of 10 hours, collecting continuously and alternatively XAS spectra at Fe (top left) and Co (top right) *K*-edges. (bottom) Evolution of the difference spectra (calculated as $\Delta I(t) = I(t)-I(t = 0)$) during the X-ray irradiation of 10 hours at Fe (bottom left) and Co (bottom right) *K*-edges.

Estimation of the Co(II) and Fe(III) contents in 1 during X-ray irradiation:

The difference spectra during X-ray irradiation (Fig. 3, $\Delta I(t) = I(t)-I(t = 0)$) are compared to the difference spectra between 295 and 125 K (Fig. 2, $\Delta I_{100\%} = I(295\ K) - I(125\ K)$). The Co(II) and Fe(III) contents are considered to be 100% at 295 K and 0% at 125 K. The Co(II) and Fe(III) contents are thus independently determined by estimating the proportionality coefficient, *p,* to scale the $\Delta I_{100\%}$ spectra ($\Delta I(t) = p\Delta I_{100\%}$) on the experimental $\Delta I(t)$ at Co and Fe *K*-edges, respectively. Fig. S5 illustrates two examples of experimental difference spectra (ΔI(1h10) for Co *K*-edge, and ΔI(1h30) for Fe *K*-edge) obtained during X-ray irradiation (in red) and the corresponding scaled $\Delta I_{100\%}$ spectra (in blue). It is worth to note that during irradiation, Co *K*-edge has always been measured before Fe *K*-edge. The same procedure has been applied for all the difference spectra, $\Delta I(t)$, shown in Figs. 3 and S5.

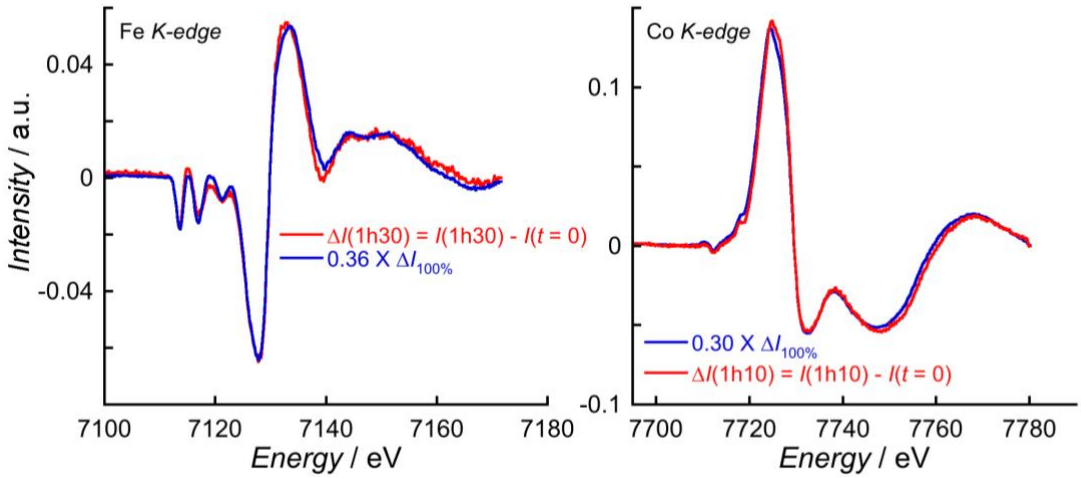

Figure S6. Selected examples of experimental difference spectra (in red; right: ΔI(1h10) for Co *K*-edge; and left: ΔI(1h30) for Fe *K*-edge) obtained during X-ray irradiation by collecting continuously and alternatively XAS spectra at Co and Fe *K*-edges. The corresponding scaled $\Delta I_{100\%}$ spectra are shown in blue at each *K*-edge.

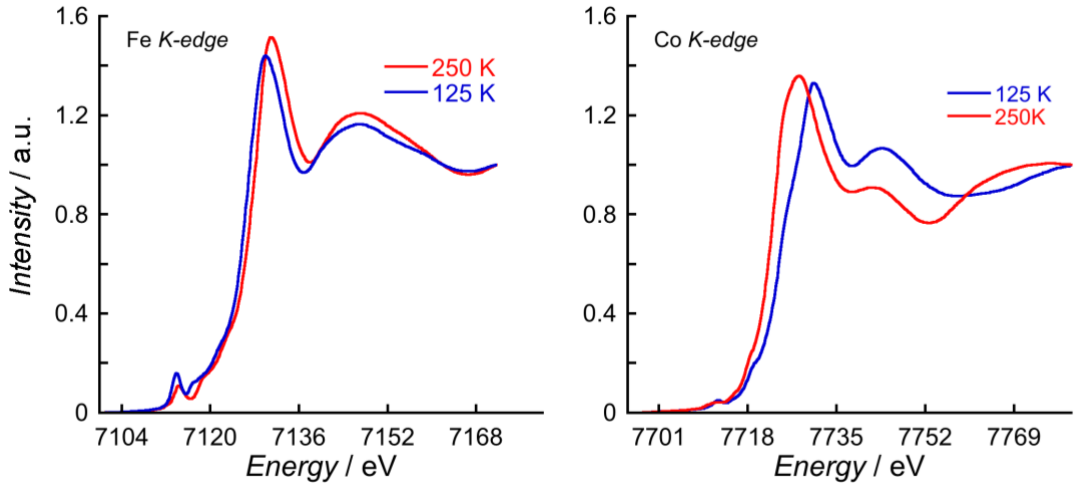

Figure S7. X-ray absorption spectra (XAS) at 250 K (red) and 125 K (blue), for the Fe (left) and Co (right) *K*-edges after 10 hours of X-ray irradiation (Figs. 3 and S5). This figure illustrates the good reproducibility and reversibility of the thermally induced electron transfer and the absence of X-ray radiation damage after extended X-ray irradiation.

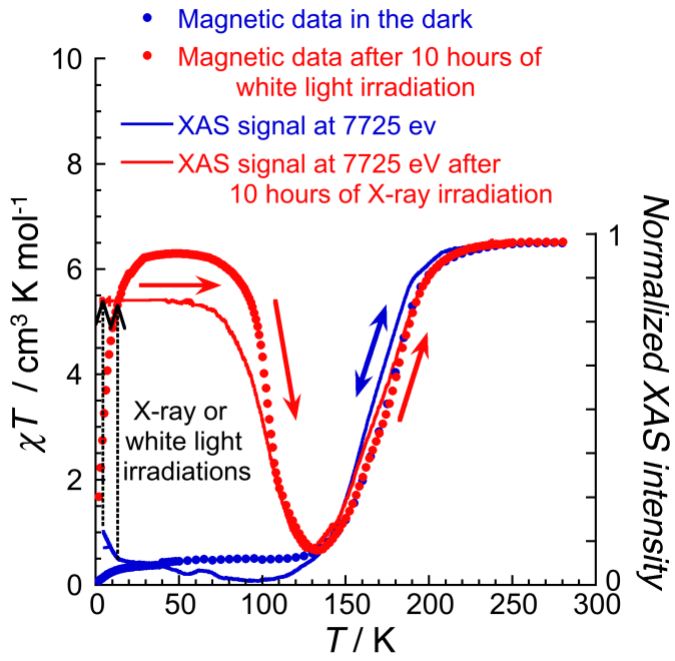

Figure S8. Comparison the temperature dependence of photomagnetic[1] and XAS data. **Photomagnetic data adapted from reference 1:** Temperature dependence of the χT product (with χ defined as the molar magnetic susceptibility and equal to *M*/*H*) for compound **1** in solid state. Blue: in the dark before irradiation at 0.5 T upon cooling, and at 1 T upon heating at 0.8 K/min; red: at 1 T upon heating at 0.4 K/min after a white light irradiation (black arrow; P = 2 mW/cm^2). **XAS data (Fig. 4):** Temperature dependence of the normalized XAS intensity at 7725 eV (Co *K*-edge) between 230 and 3 K (blue) and between 3 and 240 K (red) after 10 hours of X-ray irradiation at 3 K (black arrow). The scan rate is about 1 K min^{-1}.

References

1. D. Siretanu, D. Li, L. Buisson, D. M. Bassani, S. M. Holmes, C. Mathonière and R. Clérac, *Chem. Eur. J.*, 2011, **17**, 11704-11708.
2. A. Altomare, M. C. Burla, M. Camalli, G. Cascareno, C. Giacovazzo, A. Guagliardi, A. G. G. Moliterni, G. Polidori and R. Spagna *J. Appl. Cryst.*, 1999, **32**, 115-119.
3. G. M. Sheldrick, *Acta Cryst.*, 2008, **A64**, 112-122.
4. M. O. Krause and J. H. Oliver, *J. Phys. Chem. Ref. Data*, 1979, **8**, 329-338.
5. B. T. Thole, R. D. Cowan, G. A. Sawatzky, J. Fink and J. C. Fuggle, *Phys. Rev. B* 1985, **31**, 6856-6858.
6. F. M. F. de Groot and A. Kotani, *Core Level Spectroscopy of Solids*, *CRC Press*, Boca Raton, 2008.
7. M.-A. Arrio, S. Rossano, C. Brouder, L. Galoisy and G. Calas *Europhys. Lett.*, 2000, **51**, 454-460.
8. G. Poneti, M. Mannini, L. Sorace, Ph. Sainctavit, M.-A. Arrio, E. Otero, J. C. Cezar and A. Dei, *Angew. Chem. Int. Ed.* 2010, **49**, 1954-1957.
9. R. K. Hocking, E. C. Wasinger, F. M. F. de Groot, K. O. Hodgson, B. Hedman and E. I. Solomon, *J. Am. Chem. Soc.* 2006, **128**, 10442-10451.
10. S. F. Jafri, E. S. Koumousi, Ph. Sainctavit, A. Juhin, V. Schuler, O. Bunau, D. Mitcov, P. Dechambenoit, C. Mathonière, R Clérac, E. Otero, P. Ohresser, C. Cartier dit Moulin and M.-A. Arrio, *Inorg. Chem.*, 2016, **55**, 6980-6987.
11. M. Lundberg, T. Kroll, S. DeBeer, U. Bergmann, S. A. Wilson, P. Glatzel, D. Nordlund, B. Hedman, K. O. Hodgson and E. I. Solomon, *J. Am. Chem. Soc.*, 2007, **128**, 17121-17134.
12. V. Vercamer, M. O. J. Y. Hunault, G. Lelong, M. W. Haverkort, G. Calas, Y. Arai, H. Hijiya, L. Paulatto, C. Brouder, M.-A. Arrio, and A. Juhin, Phys. Rev. B, 2016, **94**, 245115(1-15).
13. T. E. Westre, P. Kennepohl, J. G. De Witt, B. Hedman, K. O. Hodgson and E. I. Solomon, *J. Am. Chem. Soc.*, 1997, **119**, 6297-6314.